Holographic Ghost Imaging and the Violation of a Bell Inequality

B. Jack,[1] J. Leach,[1] J. Romero,[1] S. Franke-Arnold,[1] M. Ritsch-Marte,[2] S. M. Barnett,[3] and M. J. Padgett[1]

[1]*Department of Physics and Astronomy, SUPA, University of Glasgow, Glasgow G12 8QQ, United Kingdom*
[2]*Division for Biomedical Physics, Innsbruck Medical University, A-6020 Innsbruck, Austria*
[3]*Department of Physics, SUPA, University of Strathclyde, Glasgow G4 0NG, United Kingdom*
(Received 11 May 2009; published 20 August 2009)

We demonstrate the contrast enhancement of images within a ghost-imaging system by use of nonlocal phase filters. We use parametric down-conversion as the two-photon light source and two separated phase modulators, in the signal and idler arms which represent different phase filters and objects, respectively. We obtain edge enhanced images as a direct consequence of the quantum correlations in the orbital angular momentum (OAM) of the down-converted photon pairs. For phase objects, with differently oriented edges, we show a violation of a Bell-type inequality for an OAM subspace, thereby unambiguously revealing the quantum nature of our ghost-imaging arrangement.

Ghost imaging was proposed as an illustration of the quantum correlations between pairs of photons created in spontaneous parametric down-conversion [1,2]. The photons in each pair are spatially separated, and each propagates along a distinct optical path. The optical image is revealed in the coincidences between pairs of such photons, with only limited information available in counts from either one of the detectors alone. Since the first observations more than 10 years ago [3,4], the phenomenon has remained controversial, not because of any question concerning the experiments, but on whether or not ghost imaging is solely a quantum phenomenon [5–13]. A recent analysis of this question may be found in [14]. The debate on the quantum vs classical nature of ghost imaging has lead to other interesting two-photon imaging effects using classical sources [15]. It is quantum theory that provides our best current description of light and for us the question is not whether ghost imaging is a quantum phenomenon, but rather whether the consequences of its nonclassical nature can be observed.

The first experiments on the nonlocality of entangled photons utilized optical polarization [16]. Ghost imaging, however, relates to measurements of transverse spatial modes. The spatial modes and their Fourier transform correspond to measurements of position and momentum, respectively, and hence relate to the original EPR paradox [17]. Previous experimental investigations with entangled sources show strong correlations in the near-field (position) and far-field (momentum) [7,8]. One way to determine whether these correlations are quantum in origin would be to test against a suitable Bell inequality. An experimental investigation of Bell's inequality is the standard method to test whether results can be explained through local hidden-variable theories. Violation of Bell-type inequalities have been demonstrated originally on polarization measurements [16] and subsequently on measuring correlations between spatial modes [18,19]. Crucially, previous

to this Letter, a Bell violation approach has not been applied to analyzing ghost images.

In terms of spatial modes, one can make the extension to helically-phased modes and their associated orbital angular momentum (OAM) (in analogy to the position-momentum relationship [20]). All helically-phased modes described by a phase profile $\exp(i\ell\phi)$ carry an OAM of $\ell\hbar$ per photon [21,22]. At the quantum level, OAM has been shown to be an entangled property of down-converted photon pairs [23–25].

In classical imaging, various techniques give enhanced images. Many of these techniques were developed within microscopy and include dark field and phase contrast [26]. Traditionally each technique required different objective lenses or phase filters within the microscope. However, programmable spatial light modulators (SLMs) can be incorporated into the microscope to introduce specific phase filters so that all of these imaging modes can be sequentially implemented without any change of hardware [27]. For example, the use of spiral phase plates introduces modes with OAM which can result in images with edge enhancement [28,29].

In this Letter, we apply these edge enhancement techniques to ghost imaging and show how a phase filter, nonlocal with respect to the object, leads to enhanced coincidence images. Furthermore, we are able to achieve high-contrast images, which we can interpret as a violation of a Bell inequality—thus demonstrating the quantum nature of this implementation of ghost imaging.

Our experimental system, shown in Fig. 1, is based upon a mode-locked (100 MHz) 355 nm pump source, which is weakly focussed into a 3 mm long BBO crystal, cut for degenerate type 1, noncollinear down conversion. Upon leaving the crystal, the signal and idler down-converted beams have a half-angle separation of 4°. The light in the plane of the crystal is imaged onto a phase object in the signal arm and a phase filter in the idler arm. The phase
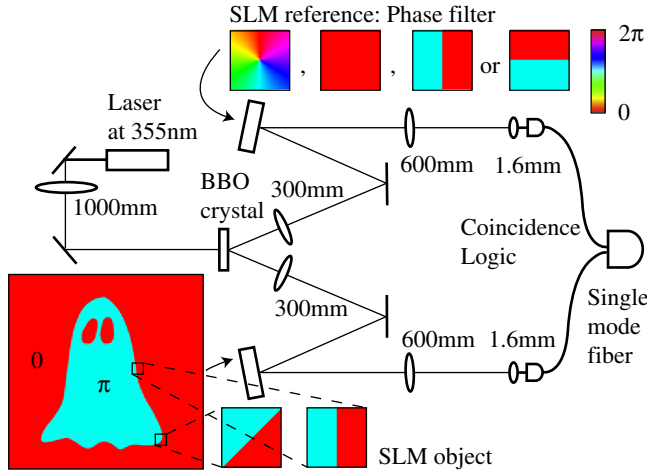
FIG. 1 (color online). Experimental setup. The phase object is stepped across the beam and imaged onto the single-mode fiber. At each position the local form of the object can be treated as a simple phase step of appropriate orientation and coincidence measurements are made for different reference holograms. The details of the experimental setup are explained in the main text.

object and phase filters are implemented by two SLMs (Hamamatsu), one in each arm. Both SLMs are then re-imaged, through 2 nm wide band-pass filters, to the input facets of single-mode optical fibers. These fibers are coupled to single-photon counter modules (Perkin Elmer), the outputs from which are fed to a coincidence counter (National Instruments). The magnification of the optics is such that the 5 μm diameter fiber facet is imaged to a 2 mm diameter spot on the SLM and then reimaged to a 300 μm diameter spot at the crystal, which is slightly smaller than the beam waist of the pump beam.

When viewed independently, both signal and idler beams are spatially incoherent [30] with a transverse mode spectrum defined by the geometry of the nonlinear crystal and the detection optics [31]. Images are produced from the correlations between the down-converted photons. The spatial resolution and contrast of such images is set by the size of the detection aperture, and in our experiment the single-mode fibers ensure both high resolution and single-mode selectivity. We are primarily concerned with helically-phased modes characterized by an $\exp(i\ell\phi)$ phase term, and modes containing a phase step, characterized by the orientation of the discontinuity; see Fig. 1.

For a down-conversion source, a precise calculation of the coincidence count is obtained by considering the back projection of one of the detected photons. The photon is back propagated through the reference filter, to the non-linear crystal, and is reflected to the object and its local detector [32]. By projecting both of these spatial modes back to the crystal, one sees that the predicted coincidence count is proportional to their overlap integral with the pump beam [33],

$$\left| \int \exp(i\ell_s\phi) \exp(i\ell_i\phi) \psi_p(r, \phi) dA \right|^2, \quad (1)$$

where $\psi_p(r, \phi)$ is the complex amplitude of the pump and ℓ_s and ℓ_i characterize the signal and idler modes. Thus, for a plane-waved pump beam, the coincidence rate is high when $\ell_s + \ell_i = 0$ and low when $\ell_s + \ell_i \neq 0$. Modes carrying a phase term of the form $\exp(i\ell\phi)$ form a complete basis set such that any object, or part thereof, can be described by an appropriate superposition of such modes.

In our system, the object is larger than the point spread function of detection, such that we see only a small portion of the object at any one time. The image is acquired by stepping the object in the transverse plane and recording the corresponding coincidence count. For a phase object, the spatial incoherence of the source means that the image derived from the object arm alone has a low contrast, see Fig. 2(b), which decreases with increasing modal bandwidth of the down conversion and detection processes.

When a spiral phase filter, with index ℓ_{ref}, is placed in the reference arm, the resulting coincidence count is proportional to the modal component of the object that corresponds to $\ell_{\text{obj}} = -\ell_{\text{ref}}$. Any part of the object described by a uniform phase corresponds to $\ell_{\text{obj}} = 0$, which gives a high coincidence count for $\ell_{\text{ref}} = 0$ and zero coincidence count for $\ell_{\text{ref}} \neq 0$. For a part of the object containing a π-phase step, an expansion in terms of $\exp(i\ell_{\text{obj}}\phi)$ gives nonzero components for $\ell_{\text{obj}} = \pm 1$. Such a phase step
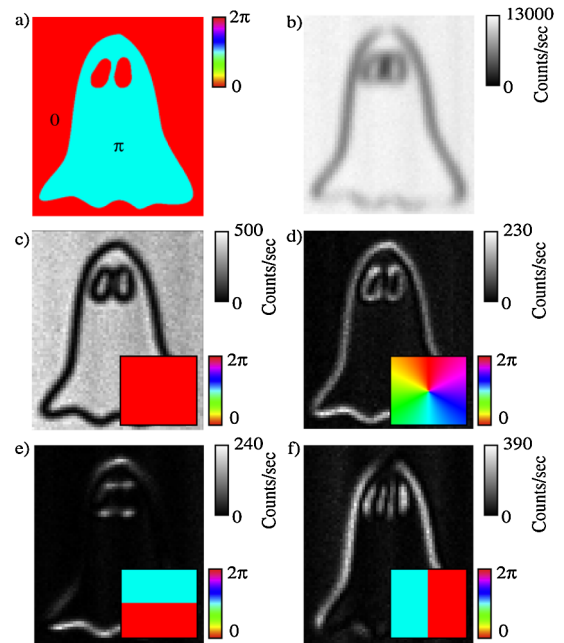

FIG. 2 (color online). (a) Phase object. (b) Single channel counts from the object detector. (c)–(f) Coincidence images of the phase object shown in (a), using reference holograms shown in insets. Note that although the object can still be discerned in (b), the edge visibility is only $\approx 2{:}1$, as compared with greater than 35:1 for the $\ell_{\text{ref}} = 0$ case (c), and 13:1 for the $\ell_{\text{ref}} = 1$ case (d).

therefore gives a high coincidence count for $\ell_{\mathrm{ref}} = \pm 1$. Hence both $\ell_{\mathrm{ref}} = 0$ and $\ell_{\mathrm{ref}} = \pm 1$ give images with high-contrast edges, but with dark edges and bright edges, respectively. A phase filter of $\ell_{\mathrm{ref}} = 0$ results in high coincidence counts wherever the phase of the object is uniform and zero coincidence at the edge; see Fig. 2(c). Also, a phase filter with $\ell_{\mathrm{ref}} = \pm 1$ results in high coincidence counts only at positions of the phase steps, giving bright edges; see Fig. 2(d). The high contrast of the images (there is no background subtraction) relies upon the spatial mode selectivity of detection and, in this case, the same images could not be obtained by using a multimode "bucket" detector in either the object or reference arm. (Note, in general, $\ell_{\mathrm{ref}} = \pm 1$ will give edge enhancement to all images irrespective of the precise height of the phase step.)

Although the coincidence images have features that are not present in images derived from the object detector alone, the correlations required to produce the image need not be uniquely quantum [14]. All that is required is conservation of OAM between the photon pairs. The signature of quantum entanglement is not that correlations exist for a particular variable, but that these correlations persist when measured in a complementary basis. In experiments based on imaging, the quantum signature is that high-contrast correlations are also observed in the diffraction pattern, without any background subtraction [7,8]. For OAM, the correlations must persist between angular momentum states and their superpositions [19]. Hence, within our imaging system, the complementary basis is a reference hologram formed from the linear superposition of $\ell = 1$ and $\ell = -1$. This superposition corresponds to a π-phase step orientated at an angle θ—determined by the phase difference, $\Delta\phi = \theta$ between the $\ell = 1$ and $\ell = -1$ modes [34]. Using this phase step as the reference hologram gives coincidence images where the contrast of the edge detection depends on the relative orientation of the edge with respect to the reference phase step; see Fig. 2(e) and 2(f).

The high contrast between parallel and orthogonal states in complementary basis sets, demonstrative of the EPR paradox, is not sufficient to distinguish between quantum and local-realistic theories. This can be achieved by violating a Bell inequality. For this, we record the coincidence rate as a function of the relative angle $\theta_A - \theta_B$ between the orientation of the edge in the object and phase step in the reference arm. Our measurements detect only superpositions of $\ell = 1$ and $\ell = -1$ and therefore our observations are sensitive only to the subspace of the OAM states; hence, the two-photon entangled state is

$$|\psi\rangle = \frac{1}{\sqrt{2}}[|1\rangle_A|-1\rangle_B + |-1\rangle_A|1\rangle_B]. \quad (2)$$

To violate a Bell inequality, the coincidence rate C must vary sinusoidally, which is predicted to be [19]

$$C = K\cos^2(\theta_A - \theta_B), \quad (3)$$

where K is a constant. Such a violation can be quantified using a Clauser-Horne-Shimony-Holt Bell-type inequality with the requirements $-2 \le S \le 2$, where

$$S = E(\theta_A, \theta_B) - E(\theta_A, \theta'_B) + E(\theta'_A, \theta_B) + E(\theta'_A, \theta'_B). \quad (4)$$

For the original work on polarization, θ_A and θ_B were the orientations of the polarizers [16], where as here they are the angles of the phase steps. $E(\theta_A, \theta_B)$ is calculated from the coincidence rates at particular orientations,

$$E(\theta_A, \theta_B) = \frac{C(\theta_A, \theta_B) + C(\theta'_A, \theta'_B) - C(\theta'_A, \theta_B) - C(\theta_A, \theta'_B)}{C(\theta_A, \theta_B) + C(\theta'_A, \theta'_B) + C(\theta'_A, \theta_B) + C(\theta_A, \theta'_B)}, \quad (5)$$

where $\theta'_{A,B} = \theta_{A,B} + \pi/2$. By imaging a circular phase object, which is much larger than the imaging point spread function, and using a π-phase step as the reference hologram, we can generate images containing all orientations of edges and are able to measure the "brightness" of the edges as a function of orientation. In this situation, our state space for the transverse mode comprises the OAM states $\ell_{\mathrm{ref}} = \pm 1$ of an equally weighted superposition. Hence we can test a Bell inequality on the $\ell = \pm 1$ subspace of transverse modes. It is known that tests on such subspaces reveal the quantum features of the full high-dimensional system [35,36]. Figures 3(a)–3(d) show images of the circular phase object with the reference hologram orientation at $0°$, $45°$, $90°$, and $135°$, respectively. The variation in count rates for each image is shown in Fig. 3(e). These curves are calculated from the azimuthal variation in count rate around the coincidence image. From these measurements, we determine the value of S to be 2.69 ± 0.10, clearly exceeding the local-hidden-variable bound of 2 and revealing the quantum nature of our ghost-imaging arrangement. It should be noted that the calculated value of S depends on the chosen radial range and in this case we average over the width of the measured signal; see the dashed lines in Fig. 3(a). The failure to reach maximal entanglement of $2\sqrt{2}$ reflects both finite fringe contrast, and possible contamination of the single-mode detection by higher order modes ($|\ell| > 1$), both of which reduce the value of S.

It is important to consider what results could be achieved if our entangled source was replaced with a classical, thermal light source. Coincident images obtained with thermal light have a finite background [6–8,14] which reduces the observable contrast to the level at which there will be no violation of Bell's inequality. An explicit demonstration of this is a potential topic for future research.

We have proposed a new form of ghost imaging, where the introduction of a phase filter into one of the arms can nonlocally modify the coincidence image such that its edges have enhanced contrast. The use of single-mode detectors means that the images have high contrast without need for background subtraction. Although similar types of images could be generated through means of a nonen-
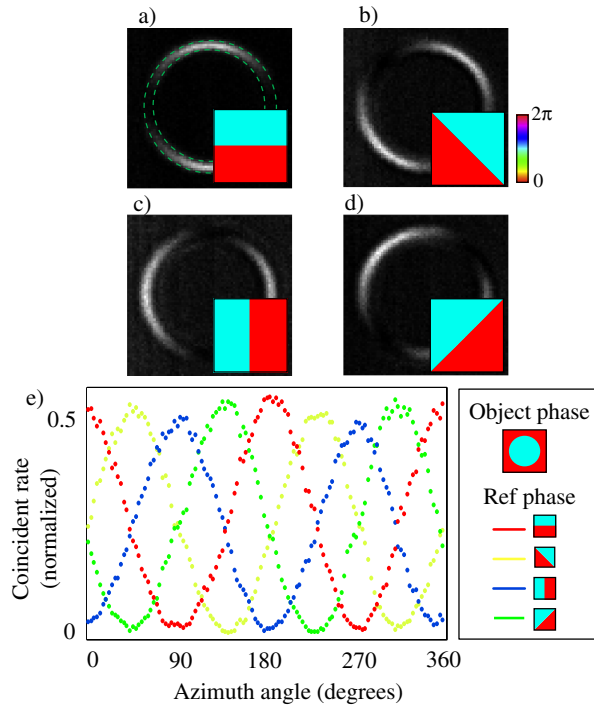
FIG. 3 (color online). (a)–(d) Coincidence images for reference orientations of 0°, 45°, 90°, and 135°, respectively. By plotting the azimuthal intensity variations in each image (e), one can see the sinusoidal pattern in coincidence, and appropriate phase shift for each analyzer hologram. The image data are averaged radially over 6 pixels and azimuthally by binning over 3°; see the dashed lines in (a).

tangled source, they would not have sufficient contrast to violate a Bell-type inequality. Indeed, satisfying or violating a Bell inequality as demonstrated in this Letter might reasonably be used to distinguish between classical and quantum ghost-imaging systems.

[1] D. N. Klyshko, Sov. Phys. JETP **76**, 1131 (1988).
[2] A. V. Belinskii and D. N. Klyshko, Sov. Phys. JETP **78**, 259 (1994).
[3] T. B. Pittman, Y. H. Shih, D. V. Strekalov, and A. V. Sergienko, Phys. Rev. A **52**, R3429 (1995).
[4] D. V. Strekalov, A. V. Sergienko, D. N. Klyshko, and Y. H. Shih, Phys. Rev. Lett. **74**, 3600 (1995).
[5] R. S. Bennink, S. J. Bentley, and R. W. Boyd, Phys. Rev. Lett. **89**, 113601 (2002).
[6] A. Gatti, E. Brambilla, and L. A. Lugiato, Phys. Rev. Lett. **90**, 133603 (2003).
[7] R. S. Bennink, S. J. Bentley, and R. W. Boyd, Phys. Rev. Lett. **92**, 033601 (2004).
[8] M. D'Angelo, Y. Kim, S. P. Kulik, and Y. Shih, Phys. Rev. Lett. **92**, 233601 (2004).
[9] G. Scarcelli, V. Berardi, and Y. Shih, Phys. Rev. Lett. **96**, 063602 (2006).
[10] A. Valencia, G. Scarcelli, M. D'Angelo, and Y. Shih, Phys. Rev. Lett. **94**, 063601 (2005).
[11] A. Gatti *et al.*, Phys. Rev. Lett. **98**, 039301 (2007).
[12] F. Ferri *et al.*, Phys. Rev. Lett. **94**, 183602 (2005).
[13] B. I. Erkmen and J. H. Shapiro, Phys. Rev. A **77**, 043809 (2008).
[14] A. Gatti, E. Brambilla, M. Bache, and L. A. Lugiato, in *Quantum Imaging*, edited by M. Kolobov (Springer, New York, 2007).
[15] R. Kaltenbaek, J. Lavoie, D. N. Biggerstaff, and K. J. Resch, Nature Phys. **4**, 864 (2008).
[16] A. Aspect, P. Grangier, and G. Roger, Phys. Rev. Lett. **49**, 91 (1982).
[17] J. C. Howell, R. S. Bennink, S. J. Bentley, and R. W. Boyd, Phys. Rev. Lett. **92**, 210403 (2004).
[18] T. Yarnall, A. Abouraddy, B. Saleh, and M. Teich, Phys. Rev. Lett. **99**, 170408 (2007).
[19] J. Leach *et al.*, Opt. Express **17**, 8287 (2009).
[20] A. K. Jha *et al.*, Phys. Rev. A **78**, 043810 (2008).
[21] L. Allen, M. W. Beijersbergen, R. J. C. Spreeuw, and J. P. Woerdman, Phys. Rev. A **45**, 8185 (1992).
[22] S. Franke-Arnold, L. Allen, and M. Padgett, Laser Photon. Rev. **2**, 299 (2008).
[23] A. Mair, A. Vaziri, G. Weihs, and A. Zeilinger, Nature (London) **412**, 313 (2001).
[24] A. Aiello, S. S. Oemrawsingh, E. R. Eliel, and J. P. Woerdman, Phys. Rev. A **72**, 052114 (2005).
[25] J. T. Barreiro, N. K. Langford, N. A. Peters, and P. G. Kwiat, Phys. Rev. Lett. **95**, 260501 (2005).
[26] E. Hecht, *Optics* (Pearson Education, Essex, United Kingdom, 2001).
[27] S. Fürhapter *et al.*, Adv. Imaging Electron Phys. **146**, 1 (2007).
[28] S. Fürhapter, A. Jesacher, S. Bernet, and M. Ritsch-Marte, Opt. Express **13**, 689 (2005).
[29] A. Jesacher, S. Fürhapter, S. Bernet, and M. Ritsch-Marte, Phys. Rev. Lett. **94**, 233902 (2005).
[30] R. Ghosh, C. K. Hong, Z. Y. Ou, and L. Mandel, Phys. Rev. A **34**, 3962 (1986).
[31] J. P. Torres, A. Alexandrescu, and L. Torner, Phys. Rev. A **68**, 050301 (2003).
[32] T. Aichele, A. I. Lvovsky, and S. Schiller, Eur. Phys. J. D **18**, 237 (2002).
[33] S. Franke-Arnold, S. M. Barnett, M. J. Padgett, and L. Allen, Phys. Rev. A **65**, 033823 (2002).
[34] M. J. Padgett and J. Courtial, Opt. Lett. **24**, 430 (1999).
[35] N. Gisin, Phys. Lett. A **154**, 201 (1991).
[36] S. M. Barnett and S. J. D. Phoenix, Phys. Lett. A **167**, 233 (1992).